OPEN

Reversal of Anchorage-Independent Multicellular Spheroid into a Monolayer Mimics a Metastatic Model

Rani Kunjithapatham[1], Swathi Karthikeyan[1], Jean-Francois Geschwind[1], Esther Kieserman[2], MingDe Lin[1], De-Xue Fu[1] & Shanmugasundaram Ganapathy-Kanniappan[1]

[1]Russell H. Morgan Department of Radiology and Radiological Sciences, [2]Microscope Facility, Johns Hopkins University School of Medicine, Baltimore, MD, USA.

Lack of an *in vitro* model of metastasis has been a major impediment in understanding the molecular regulation of metastatic processes, and identification of specific therapeutic targets. We have established an *in vitro* model which displayed the signatures of metastatic phenotype such as migration, invasiveness, chemoresistance and expression of cancer stem-cell markers. This *in vitro* model was developed by the induction of reversal of multicellular spheroids that were generated by anchorage-independent growth. *In vivo* data further validated the metastatic phenotype of the *in vitro* model. Besides delineating the molecular events of metastasis, this model could also improve the screening efficiency of antimetastatic agents.

Cancer-related high mortality rate and poor prognosis are often attributed to the aggressive phenotype known as metastasis[1]. Although our understanding on the process of metastasis has significantly advanced in the recent past, the development of an effective therapeutic for metastasis remains elusive. Identification of a sensitive molecular target requires a detailed characterization of the regulatory networks of metastatic-cascade. This in turn relies on an ideal *in vitro* model that represents all the known properties of metastatic cancer. Current metastatic models rely to a great degree on *in vivo* methods such as intraperitoneal, intravenous or subcutaneous delivery of cancer cells followed by the investigation of tumorigenesis at distal organs[2,3]. These methodologies are very useful to characterize the tumorigenic potential of cancer cells and the nature of micro-environment that facilitates tumor formation. However, these approaches circumvent or evade the key features of metastatic cascade such as invasion, migration, and epithelial-mesenchymal transition (EMT). Due to the omission of such initial steps of metastatic cascade it is plausible that potential molecular targets may be missed.

On the other hand, *in vitro* models to mimic metastasis largely rely upon the "Boyden chamber" design, and several modifications of it, which demonstrate the invasion of cancer cells[4]. Although the assay in general represents one of the salient features of metastasis, it relies heavily on local-invasion which doesn't depend on EMT and cancer-stemness/tumorigenic potential that are frequently witnessed in metastatic cells. A recent development in the creation of an *in vitro* system is the generation of three dimensional (3D) culture with the aid of extracellular matrix (ECM) or ECM-like materials that facilitate cellular aggregation and prevent attach-ment of cells to the adhesive-basement of the culture vessel. Such 3D cultures, also referred as multicellular spheroids (MCS), provide many advantages over the conventional 2D culture (monolayer)[5]. From the metastasis perspective, although, the 3D architecture mimics the *in vivo* tumor and has been known to possess cancer stem cell markers and the "potential" for metastasis[6], the manifestation of metastatic phenotype remains unclear. Furthermore, potential concerns and technical issues related to the adhesion-complexes of 3D culture and their impact on the biology of cancer cells have also been reviewed[7]. Thus there is a critical need for an ideal *in vitro* model that represents distinctive features of metastasis such as migration/invasion, chemoresistance and cancer stem cell-like potential.

Results

MCS generated without the use of exogenous gel-like materials (e.g. matrigel) spontaneously reversed into monolayer under normal culture condition. The reversal process involved migration of cells from the spheroidal structure towards the base of the MCS. Fig. 1 (upper panel) shows a schematic representation of the conventional monolayer cells with tumorigenic population, followed by the recent advancement over the monolayer culture
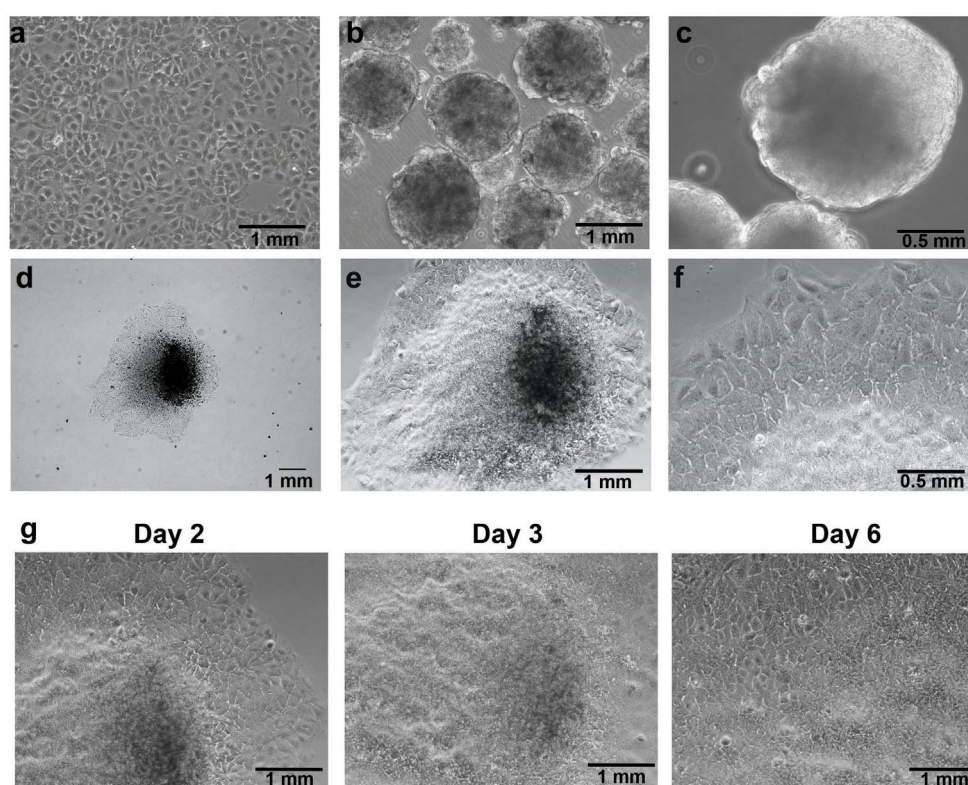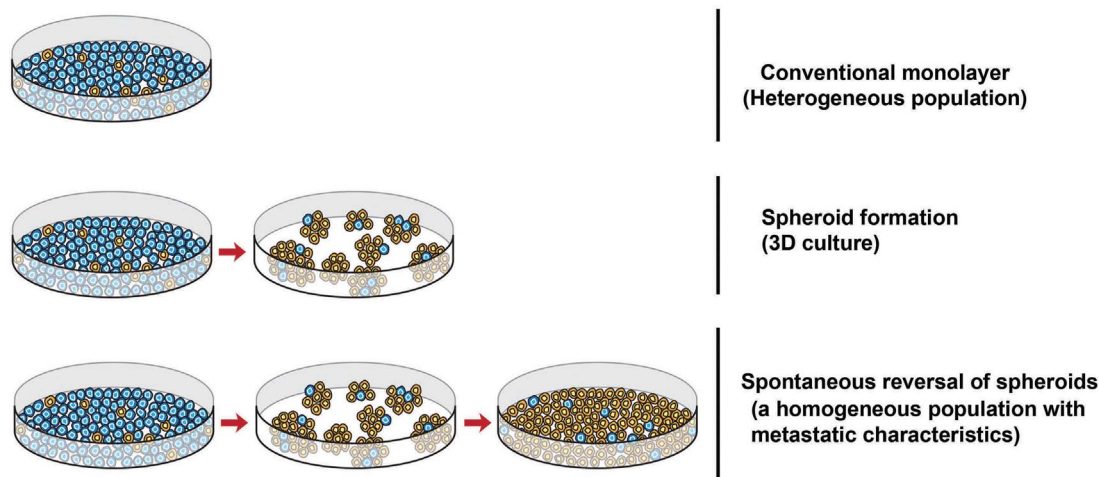
Figure 1 | Development of anchorage-independent multicellular spheroids and induction of reversal into monolayer. Upper panel: A schematic showing current *in vitro* models and the proposed *in vitro* model. Lower panel: (a) The parental cell line, Huh7 as monolayer. (b,c) Anchorage-independent growth of multicellular spheroids shown at low (b) and high magnifications (c). (d–f) Induction of reversal of a spheroid into monolayer at increasing magnifications. (g) Progressive reversal of a spheroid over few days to reach complete reversal.

resulting in 3D MCS, and the proposed model of induction of reversal of spheroids. We subjected parental populations of cells to ultra-low attachment culture conditions necessitating an anchorage-independent growth to form MCS (Fig. 1b–c). One of the advantages of MCS that are grown under anchorage-independence is the selection of clonogenic- or aggressive-phenotypic cells while eliminating the proliferative but non-malignant cells that often dominate any heterogeneous parental cell line (Supplementary Fig. S1).

Following the generation of MCSs by anchorage-independence, we next induced the <u>r</u>eversal of <u>s</u>pheroids (for simplicity here after referred as *rs*) by transferring them into normal (adhesive) culture condition (Fig. 1d–f). During the reversal process, cells were observed to migrate in a "down-hill" fashion from the vertical top

axis of the spheroid to its base which is close to the attachment/adhesive-surface, but in a direction away from the spheroid-base (Fig. 1g). These events were consistent and verified in multiple cultures of the Huh7 cell line (Supplementary Fig. S2). The complete downward migration of cells from the vertical axis (top) to form the *rs*-monolayer (by reversal) required ~7 days and it primarily depended upon the size of the spheroid and type of cancer cells. Interestingly, during the process of migration cells exhibited typical features of motility such as fillopodia or pseudopodia like protrusions prior to migration (Supplementary Fig. S3).

Next, we evaluated if this reversal in morphology correlated with metastatic genotype. Data from quantitative RT-PCR (qPCR) analysis showed a marked increase in the expression of cancer-stem cell

(CSC) markers (ALDH1A1, EpCAM, CD133, CD90, CXCR4, NANOG), as well as genes associated with drug resistance (ABCG2) and invasiveness (TGLN, Snail1, CDH12) in *rs*-monolayer cells (Fig. 2). We then verified if the elevation in the mRNA level of genes associated with metastasis or invasion correlated with the phenotypic expression of corresponding proteins in *rs*-monolayer. Immunofluorescent analysis of transgelin, a protein associated with migration, showed a marked increase in its expression in the *rs*-monolayer of multiple cell lines such as Huh7, SK-Hep1 and MCF-7 indicating the enrichment of metastatic cells in *rs*-population (Fig. 3; Supplementary Fig. S4). Similarly, the expression of the EMT marker, vimentin, is increased in *rs*-monolayer despite being reversed to epithelial-monolayer phenotype thus demonstrating that the markers of EMT are retained in the *rs*-monolayer population (Fig. 4). Together, the mRNA expression level as well as the phenotypic expression of corresponding proteins indicate that the *rs*-monolayer population is highly metastatic than the parental population.

Functional analysis revealed that the invasive capacity of *rs*-monolayer is markedly high compared to the parental population. Data from the invasion assay demonstrated that the *rs*-monolayer has higher number of invading cells than the parental cell line indicating the enrichment of metastatic population in *rs*-monolayer (Fig. 5a,b). Analysis of matrix metallo proteases (MMP) activity by zymogram and its expression by immunoblot showed increased activity and an elevation in the level of expression (Fig. 5c). This corroborated the higher invasive-ability of *rs*-monolayer cells compared to the parental population. Thus, *rs*-monolayer exemplifies migratory and invasive characteristics that are integral components of metastatic processes. Further, the aggressive metastatic phenotype was also complemented by the expression level of cancer-stem cell (CSC) markers such as CXCR4, EpCAM and CD133. Immunofluorescent analysis showed that the *rs*-monolayer population exhibit higher expression level of CSC markers compared to their corresponding parental population indicating the enrichment of CSC-like cells in the *rs*-monolayer (Fig. 6, Supplementary Fig. S5).

Next we investigated if the metastatic phenotype exhibited by *rs*-monolayer also correlated with any differential sensitivity to anticancer agents. In accordance with the qPCR data (Fig. 2), the expression level of ABCG2, a regulator of drug-efflux that plays a pivotal role in chemoresistance, showed a marked increase in *rs*-monolayer (Fig. 7a, Supplementary Fig. S6). To validate that the increased expression of ABCG2 affects drug sensitivity we treated *rs*-monolayer and parental monolayer cells of *luc*-Huh7 to a glycolytic inhibitor, 3-bromopyruvate. The data show that the *rs*-monolayer cells require a higher concentration of drug to achieve the IC$_{50}$ indicating a decrease in sensitivity (Fig. 7b). Preliminary analysis of the chemosensitivity using BIOLOG's phenotypic microarray also confirmed marked variation in response to different anticancer agents (Supplementary Fig. S7). Data showed that out of 72 anticancer agents only 27 had any effect on any form of *luc*-Huh7 cells (parental or *rs*), in which parental monolayer cells were more sensitive to 21 agents while the reversed spheroid cells were more sensitive to only 6 agents. Thus, *rs*-population in general possesses differential drug sensitivity than the parental cell line.

Next we validated the tumor initiation capacity of *rs*-cells *in vivo*. Data from animal imaging showed that intraperitoneal injection of *rs*-monolayer formed multiple nodules compared to the parental cell line (Fig. 8). This demonstrated that *rs*-monolyaer cells have higher seeding or tumor initiation capacity, a typical feature of metastatic cancer.

Discussion

Results of the current study demonstrate that reversed-spheroid population possesses aggressive phenotypic characteristics such as invasion, cancer stem cell markers and chemoresistance. Clinically, these salient features are attributed to poor prognosis and therapeutic challenges[8]. Although MCS of cancer cells have been known to possess these aggressive properties, until this report there is no documentation of the preservation or propagation of such malignant (metastatic, chemoresistant and cancer stem cell-like) phenotype after reversal into a monolayer. In other words, we demonstrate that the malignant (EMT, CSC, metastatic) characteristics of MCS are maintained even after the reversal of phenotype into a monolayer. Further this also indicates that the MCS generated by ultra-low attachment culture condition rather than using a supporting med-
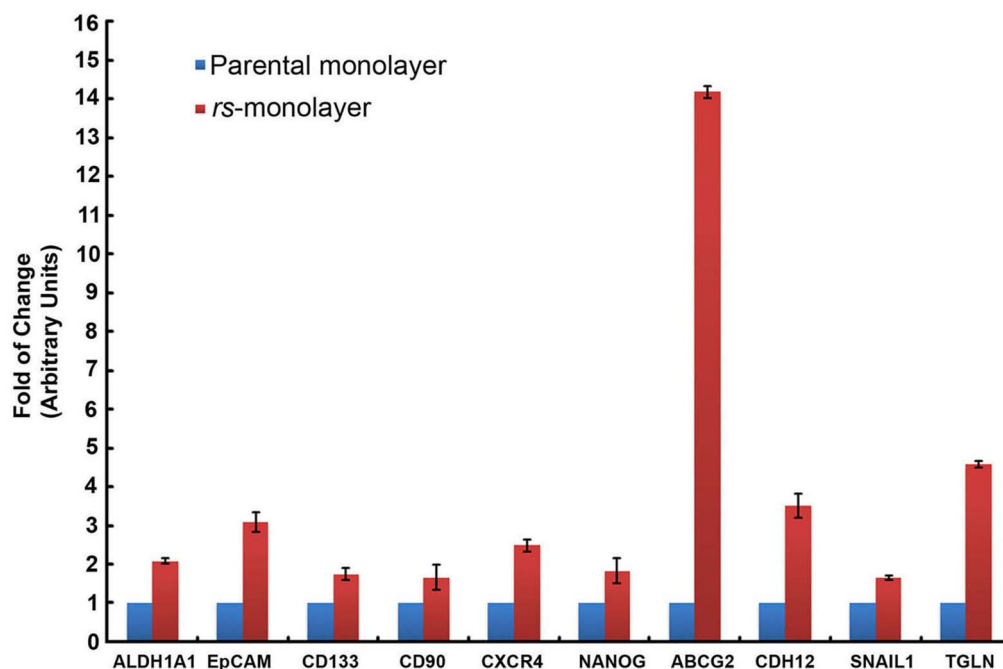

Figure 2 | Upregulation of metastatic genes in *rs*-monolayer population. qPCR showing an increase in the expression level of markers of CSC (ALDH1A1, EpCAM, CD133, CD90, CXCR4, NANOG), drug resistance (ABCG2), EMT (CDH12, SNAIL1) and invasion (TGLN) in *rs*-monolayer.
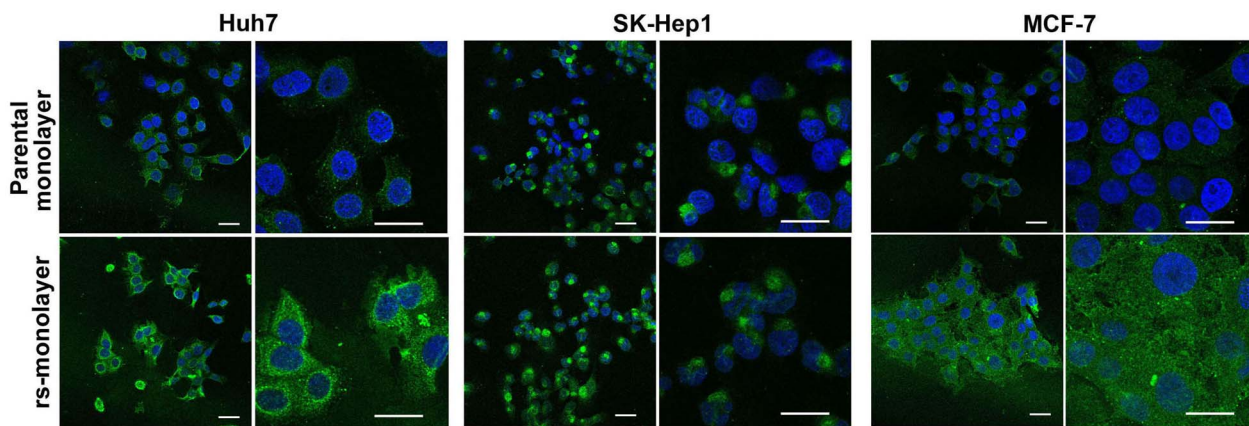
Figure 3 | Overexpression of transgelin in *rs*-monolayer population. Immunofluorescent images showing a marked increase in the expression of transgelin in *rs*-monolayer compared to the parental population in multiple cell lines. Scale bar represents 20 μm.

ium (e.g. matrix) in fact selected metastatic, aggressive cells. This is further supported by the observation that not all cells formed the MCS, and many of them did not survive the anchorage-independent condition resulting in cell death.

The reversal of MCS also circumvents some of the concerns related to spheroids under 3D culture. For example, the tumor spheroids have been known to develop chemical gradients (e.g. of oxygen, nutrients, and catabolites) at diameters between 200 and 500 μm with a central secondary necrosis typically established at sizes >500 μm[5]. While this mimics an *in vivo* tumor, from the perspective of metastasis it remains unknown whether the central necrotic core and any chemical or oxygen gradients can impact any of the metastatic properties of these cells. Moreover, *in vivo*, tumor vasculature plays a pivotal role in the delivery of required nutrients, and this is achieved through neo-angiogenesis[9]. In fact, the angiogenic phenomenon of tumor cells is so prominent that angiogenic inhibitors including anti-VEGF molecules have been intensely pursued as potential therapeutics[10,11]. *In vitro*, in the spheroids the lack of an angiogenic or vascular system confounds cellular characteristics especially under 3D, anchorage-independent culture condition.

Thus, reversal of spheroid cells into a monolayer facilitates typical epithelial phenotype but with the integration of metastatic signatures. Further, EMT is one of the early steps of initiation of metastatic processes[12]. As EMT is a critical determinant of tumor cell dissemination any 3D model of cancer cells should integrate the process of EMT[13]. Thus our approach to develop MCS solely based on anchorage-independent growth without the use of support materials (e.g. collagen or matrigel) not only induces EMT but also minimizes
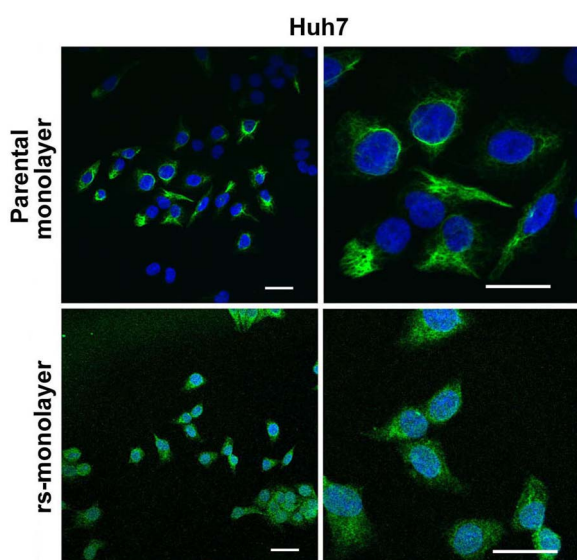

Figure 5 | *rs*-monolayer cells are highly invasive than the parental population. (a) An invasion assay showing *rs*-Huh7 cells have higher invasiveness compared to the parental population. (b) Histogram shows the percentage of migration, * indicates the p-value from statistical analysis and (c) the immunoblot and zymogram show an increase in the expression and activity of MMPs, respectively in *rs*-monolayer population. Numbers at the bottom of the zymogram image are densitometry quantifications of respective signals. The square-boxes bordering the gel image in the immunoblot as well as the zymogram gel indicate the area of the image cropped from the original blot and gel, respectively. The uncropped original images of the immunoblot (Supplementary Fig. S8) and zymogram gel (Supplementary Fig. S9) are provided in the "supplementary information".

Figure 4 | Overexpression of vimentin in *rs*-monolayer population. Immunofluorescent images showing a marked increase in the expression of vimentin, an EMT marker, in the *rs*-monolayer compared to the parental population of Huh7 cells. The right panel represents a higher magnification of the corresponding left panel. Scale bar represents 20 μm.
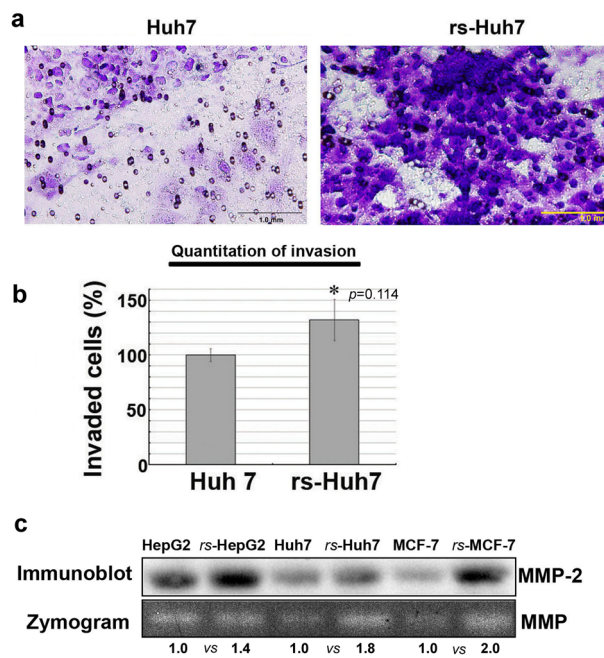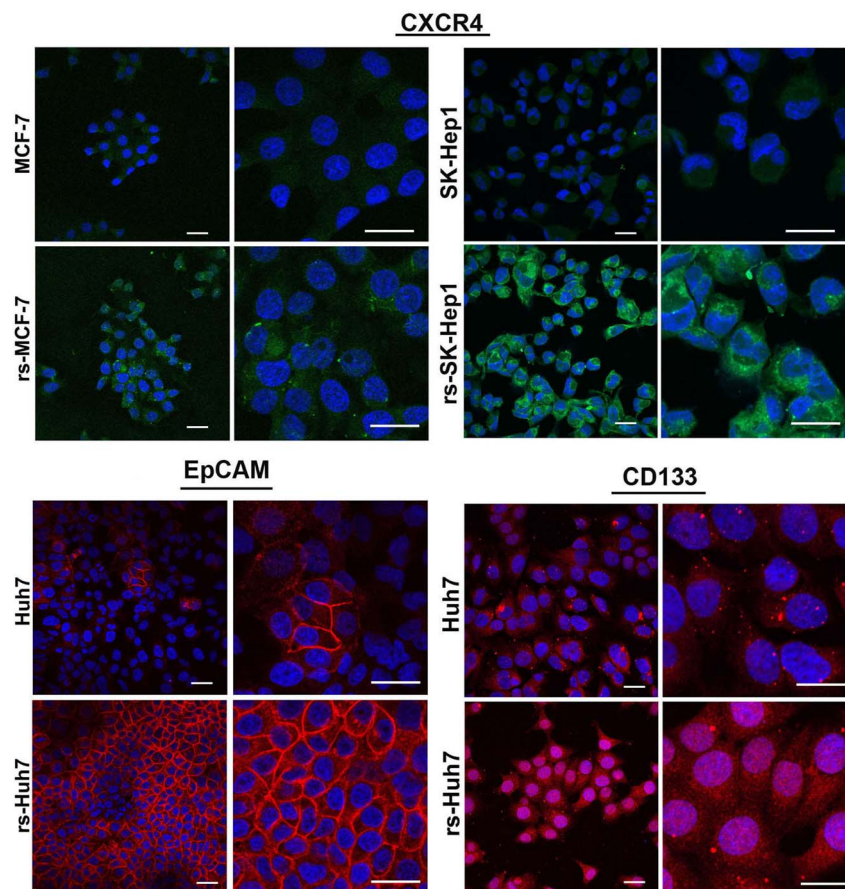
Figure 6 | Overexpression of cancer-stem cell markers in *rs*-monolayer population. Immunofluorescent images showing a marked increase in the expression of CSC markers such as CXCR4, EpCAM and CD133 in *rs*-monolayer cells compared to the parental population. Scale bar represents 20 μm.

undesirable effects, if any, that could be related to the supporting matrices.

Several studies have demonstrated that CD133 positive cells have stem cell-like features in various cancers[14,15] and it is increasingly evident that CSCs play a pivotal role in tumor metastasis[16]. Similarly, CXCR4, a receptor for chemokine SDF1, has been suggested as a critical factor for the metastatic potential of CSCs and tumor invasion[17]. The metastatic ability of CSCs has been attributed to the expression of transgelin as well. In fact, it is suggested that transgelin may replace the twist protein as a key regulator of TGF-beta signaling in at least Huh7 tumorigenic cells undergoing EMT. It is well known that EMT is characterized by the combined loss of epithelial cell junction proteins such as E-cadherin and the gain of mesenchymal markers such as vimentin[18]. Besides, recent data also establish that most malignant cells transition from EMT, and such EMT driven cells are more invasive and resistant to therapy[19]. Thus upregulation of multiple CSC markers and EMT genes in *rs*-mono-layer indicate that the aggressive phenotype acquired during the generation of anchorage-independent MCS are preserved or maintained in the reversal process as well.

Chemoresistance is a common and frequently witnessed property of metastatic cancers. Clinically, as metastatic cells are known to be resistant to cancer therapies[20], we next investigated if the *rs*-mono-layer has differential sensitivity to anticancer agents. Flow cytometry analysis further confirmed an increase in ABCG2 expressing cells (data not shown). Nevertheless, *in vivo* data unequivocally demonstrate that tumor initiation capacity of *rs*-monolayer cells is markedly higher than the parental population. In summary, the *rs*-monolayer incorporates clonogenic (colonies or spheroids) capacity, migratory and invasive properties along with chemoresistance

suggestive of all the metastatic characteristics to investigate its biology and regulation. This *in vitro* model of metastasis could be valuable in understanding the molecular regulation of metastatic cascade which in turn could provide insights into potential therapeutic targets.

Methods

Cell culture, chemical and reagents. Human hepatocellularcarcinoma (HCC) cell lines HepG2, Hep3B and SK-Hep1 were obtained from the American Type Culture Collection (ATCC) (Manassas, VA, USA). Huh7 cells were kindly provided by Dr. James Hamilton of the Gastroenterology & Hepatology department. The MCF-7 cells were obtained from ATCC (USA). The HCC cell lines SK-Hep1, HepG2, Hep3B were maintained in modified Eagle's medium (Life Technologies Inc., Grand Island, NY, USA) supplemented with 10% fetal bovine serum (FBS) (Thermo Scientific Hyclone Inc., Waltham, MA, USA), and 1% antibiotics, penicillin and streptomycin, sodium bicarbonate and sodium pyruvate (Gibco, Carlsbad, CA, USA). Huh7 cells were cultured in RPMI medium (Life technologies) with 10% FBS and 1% antibiotics. MCF-7 cells were cultured in modified Eagle's medium (Life Technologies) supplemented with 0.01 mg/ml bovine insulin, in addition to 10% FBs and 1% antibiotics.

Anchorage-independent growth and induction of reversal of multicellular spheroids (MCSs). To generate MCS from a heterogeneous parental population, cells growing log phase were seed in ultra-low attachment 6-well plates (Corning Inc. PA, USA) and cultured in complete growth medium at 37°C and 5% CO_2. No gel matrix or matrigel-like materials were used. Cells that survived this anchorage-independent condition aggregated and formed spheroids whereas cells that could not survive this selection pressure died and were floating as loose independent bodies. The spheroids generated in such ultra-low attachment culture conditions were separated from dead or unhealthy (based on the cellular morphology) cells and cultured further. To induce reversal of spheroid cells, the MCS was aseptically transferred to regular culture dish that supports adhesion of epithelial cells. Cells were allowed to migrate from the spheroid into the surface of the dish, and media was changed as may be necessary. Once the spheroid has completely reversed to monolayer the cells were trypsinized and propagated as per regular cell culture conditions.
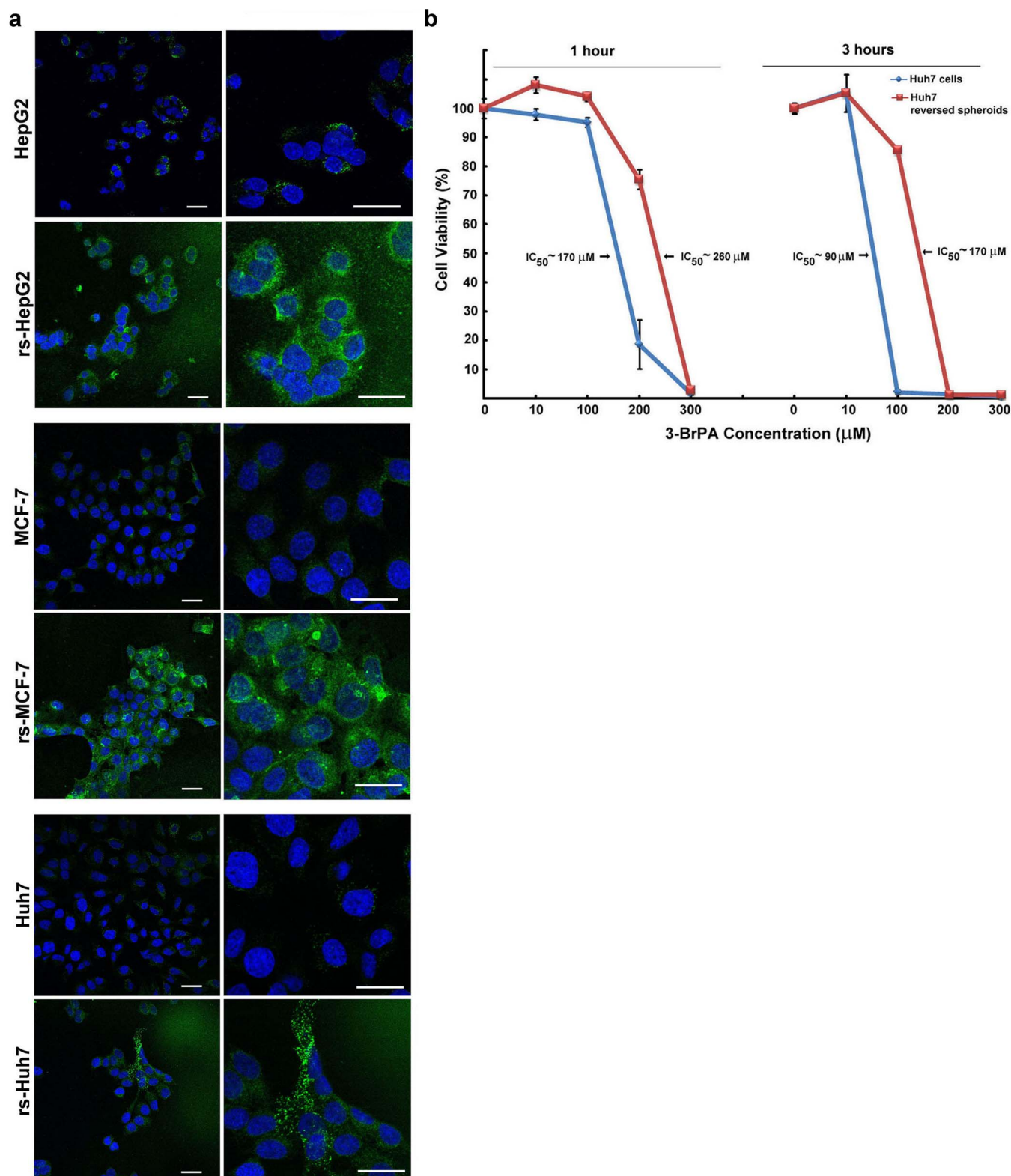
Figure 7 | Chemoresistance in *rs*-monolayer population. (a) Immunofluorescent images showing a marked increase in the expression of ABCG2, a chemoresistant phenotype, in *rs*-monolayer cells compared to the parental population in multiple cell lines. (b) Difference in the chemosensitivity of parental and *rs*-monolayer population of Huh7 cells to the antiglycolytic agent 3-BrPA. An increase in IC$_{50}$ of *rs*-monolayer cells compared to the parental population indicate the requirement of higher concentration of 3-BrPA to achieve similar toxicity. Scale bar represents 20 μm.

Generation of *luc*-Huh7 cells for phenotypic microarray (PMM) analysis. For PMM array studies, the luciferase reporter plasmid pcDNA 3.1-cytomegalovirus-firefly luciferase was provided by Martin Pomper that was initially generated in Sam Gambhir's laboratory as described[21]. Huh7 cells stably expressing *luciferase* gene were generated by transfecting them with pcDNA 3.1-cytomegalovirus-firefly luciferase plasmid by using a transfection agent (TurboFectin 8.0; OriGene Technologies), followed by clonal selection with G418 (Invitrogen, Grand Island,NY) containing growth medium. Clones expressing highest luciferase activity were selected and used for further studies. For simplicity, these stable cells will be referred hereafter as *luc*-Huh7.
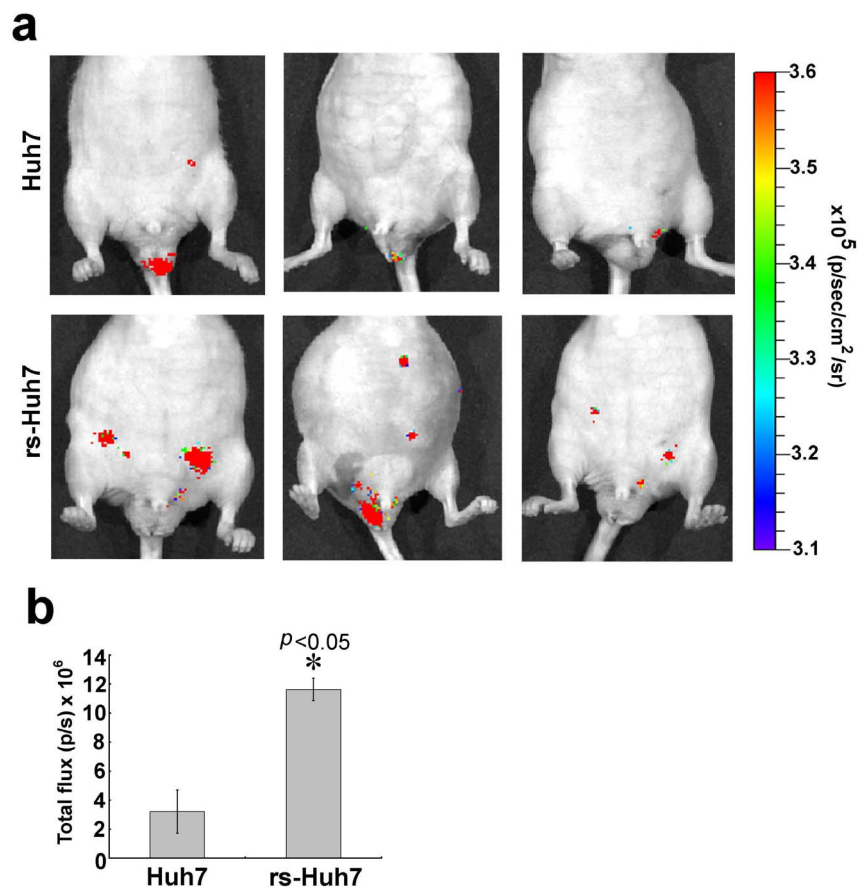
Figure 8 | Tumor initiation by *rs*-monolayer cells. (a) *Luc*-Huh7 cells were injected intraperitoneally and the tumor initiation was monitored by BLI as described in the "Materials and Methods" section. A representative of three mice images were shown for each group. (b) Bar diagram shows the mean ± SD of five mice per group. * indicates the p-value from statistical analysis.

qRT-PCR. Gene expression analysis was performed by using quantitative real-time polymerase chain reaction with a sequence detection system (ABI 7900HT; Applied Biosystems, Bedford, MA, USA) and a mix (SYBR Green PCR Master Mix; Applied Biosystems). In brief, total RNA was extracted and cDNA was synthesized as described previously[22]. The complementary DNAs thus synthesized were subjected to quantitative real-time polymerase chain reaction for specific gene expression analysis. The primers used for respective gene amplification were synthesized by RealTimePrimers.com (Elkins Park, PA, USA):

The primers used were as follows: 5′-TTGTTCCTGGTTATGGGCCT-3′ (forward) and 5′-TCCAGTTTGGCCCCTTCTTT-3′ (reverse) for ALDH1A1, 5′-TAA-AAGTTTGCGGACTGCAC-3′ (forward) and 5′-GCCACATCAGCTATGTCCAC-3′ (reverse) for EPCAM, 5′-CCTCTGGTGGGGTATTTCTT-3′ (forward) and 5′-CAGTTTCCGACTCCTTTTGA-3′ (reverse) for PROM1, 5′-AGGAAGCC-TCAAGTTCCAGT-3′ (forward) and 5′-AAAAGACAGCCAGAGGTGTG-3′ (reverse) for THY1, 5′-GGTGGTCTATGTTGGCGTCT-3′ (forward) and 5′-TGG-AGTGTGACAGCTTGGAG-3′ (reverse) for CXCR4, 5′-ACCTACCTA-CCCCAGCCTTT-3′ (forward) and 5′-CATGCAGGACTGCAGAGATT-3′ (reverse) for NANOG, 5′-TAAAGTGGCAGACTCCAAGG-3′ (forward) and 5′-TTGTTCGTCCCTGCCTTAGAC-3′ (reverse) for ABCG2, 5′-TGGATGG-ACCTTATGTTGCT-3′ (forward) and 5′-AACACCTGTCTTGGGATCAA-3′ (reverse) for CDH12, 5′-ACCCCACATCCTTCTCACTG-3′ (forward) and 5′-TACAAAAACCCACGCAGACA-3′ (reverse) for SNAI1 and 5′-GCAGTCC-AAAATCGAGAAGA-3′ (forward) and 5′-ACCAGCTTGCTCAGAATCAC-3′ (reverse) for TAGLN. The internal control primer set 18S was used (Applied Biosystems).

Invasion Assay. Invasion assay was performed using the CytoSelect Invasion assay kit from Cell Biolabs Inc (San Diego, CA, USA). The assay was performed as per manufacturer's instructions and at the end of 24 hours of invasion, cells were stained and microscopic images were captured prior to the colorimetric quantification.

Gelatin zymography for matrix metalloproteinase (MMP) activity. The level of MMP activity in the conditioned medium of parental cell lines as well as *rs*-monolayer population was quantified by gelatin zymography. Protein (7.5 μg) samples from the conditioned media of respective cell lines were subjected to zymography using 10% gelatin-zymogram gel (Invitrogen, CA). The staining procedures were followed as per the supplier's instructions. In brief, at the end of electrophoresis, the gel was incubated in zymogram renaturation buffer for 30 minutes at room temperature, followed by an overnight incubation with the zymogram developing buffer at 37°C or room temperature. Next, the gel was stained with colloidal coomassie blue followed by destaining. The MMP activity was visualized as clear bands.

Immunostaining and immunoblotting. Phenotypic analysis of metastatic markers was performed using immunodetection of specific targets followed by the acquisition of images in a confocal microscopy. In brief, the cells were grown in Lab-Tek II chamber slides (Thermo Fisher Scientific Inc. PA, USA) containing appropriate growth medium. They were fixed with 4% formaldehyde for 10 minutes, rapidly rehydrated with phosphate-buffered saline (PBS) and permeabilized with 0.5% Triton X-100 solution in PBS.

Immunostaining protocols were followed as per antibody suppliers' instructions, and the DAPI (Invitrogen, CA) nuclear stain was used as the counter-stain. In methods where non-conjugated primary antibodies were used corresponding secondary antibodies with either FITC (anti mouse, Sigma Inc., USA) or PE conjugate (anti-rabbit, Cell Signaling Technology, Boston, MA, USA) were used as per suppliers' instructions. Transgelin was stained with mouse monoclonal antibody (Santa Cruz Biotechnology Inc., CA), vimentin was stained with Alexa Fluor conjugated rabbit monoclonal antibody (Cell signaling Technology Inc.), CXCR4 was stained with mouse monoclonal antibody (Santa Cruz Biotechnology Inc.) EpCAM was stained with Alexa Fluor conjugated mouse monoclonal antibody (Cell Signaling Technology Inc.) and CD 133 was stained with rabbit monoclonal antibody (Cell Signaling Technology Inc.) and ABCG2 was stained with mouse monoclonal antibody (Santa Cruz Technology Inc.). The slides were mounted with ProLong Gold anti-fade mounting media (Invitrogen) before microscopic analysis. Images were Fluorescent images of immunostained slides were acquired with Zeiss 510 Meta LSM Confocal Microscope at the Microscope facility, Johns Hopkins School of Medicine. The size of images was adjusted across all pictures using Adobe Photoshop software for better clarity in the final figures.

Immunoblotting of MMP-2 was performed using rabbit monoclonal antibody (Cell Signaling Technology Inc.). In brief, ~7 μg of samples from the conditioned media of various cells lines were electrophoretically resolved on 4–12% Bis-Tris gel (Invitrogen) with MOP-SDS buffer and blotted onto PVDF membranes (Bio-Rad) and blocking and detection were performed as described before but using the specific MMP-2 antibody. Immune complexes were visualized by ECL-detection kit (GE Health Care).

Chemosensitivity assay. Assessment of the chemosensitivity of parental cell population and *rs*-monolayer population was performed using the antiglycolytic agent, 3-bromopyruvate (3-BrPA). In brief, cells were plated in 96-well plates the day before treatment. Analysis of cell viability following the addition of 3-BrPA was performed as described[22].

Animal experiments. Animal studies were performed as approved by the Johns Hopkins University Animal Care and Use Committee. The methods or procedures of all animal were carried out in accordance with the approved guidelines of the institution. For *in vivo* experiments, 4–5-week-old male athymic nude mice (body weight, 25–30 g) were used (Crl:NU-Fox[n1/nu] strain; Charles River Laboratory, Germantown, Md). Mice were randomly devided in to two groups of 5 mice each. Tumor initiation was investigated by intraperitoneal injection of either heterogenous population (group-1) or *rs*-population (group-2) of *luc*-Huh7 cells (5×10^6 cells/mouse). Tumor initiation or growth was monitored by bioluminescence imaging.

Statistical analysis. *In vitro* data from at least three independent experiments performed in triplicate are presented as the mean ± standard error (SEM). Comparison of BLI data were performed using one way analysis of variance (ANOVA).

1. Sethi, N. & Kang, Y. Unravelling the complexity of metastasis - molecular understanding and targeted therapies. *Nat. Rev. Cancer.* **11**, 735–748 (2011).
2. Francia, G., Cruz-Munoz, W., Man, S., Xu, P. & Kerbel, R. S. Mouse models of advanced spontaneous metastasis for experimental therapeutics. *Nat. Rev. Cancer.* **11**, 135–141 (2011).
3. Nguyen, D. X., Bos, P. D. & Massague, J. Metastasis: from dissemination to organ-specific colonization. *Nat. Rev. Cancer.* **9**, 274–284 (2009).
4. Albini, A. *et al.* A rapid in vitro assay for quantitating the invasive potential of tumor cells. *Cancer Res.* **47**, 3239–3245 (1987).
5. Hirschhaeuser, F. *et al.* Multicellular tumor spheroids: an underestimated tool is catching up again. *J. Biotechnol.* **148**, 3–15 (2010).
6. Liao, J. *et al.* Ovarian cancer spheroid cells with stem cell-like properties contribute to tumor generation, metastasis and chemotherapy resistance through hypoxia-resistant metabolism. *PLoS One* **9**, e84941 (2014).
7. Harunaga, J. S. & Yamada, K. M. Cell-matrix adhesions in 3D. *Matrix Biol.* **30**, 363–368 (2011).
8. Perona, R., Lopez-Ayllon, B. D., de Castro Carpeno, J. & Belda-Iniesta, C. A role for cancer stem cells in drug resistance and metastasis in non-small-cell lung cancer. *Clin. Transl. Oncol.* **13**, 289–293 (2011).
9. De Paepe, B. Anti-angiogenic agents and cancer: current insights and future perspectives. *Recent. Pat. Anticancer Drug Discov.* **4**, 180–185 (2009).
10. Gerstner, E. R. *et al.* VEGF inhibitors in the treatment of cerebral edema in patients with brain cancer. *Nat. Rev. Clin. Oncol.* **6**, 229–236 (2009).
11. Ivy, S. P., Wick, J. Y. & Kaufman, B. M. An overview of small-molecule inhibitors of VEGFR signaling. *Nat. Rev. Clin. Oncol.* **6**, 569–579 (2009).
12. Thiery, J. P. Epithelial-mesenchymal transitions in tumour progression. *Nat. Rev. Cancer.* **2**, 442–454 (2002).
13. Kimlin, L. C., Casagrande, G. & Virador, V. M. In vitro three-dimensional (3D) models in cancer research: an update. *Mol. Carcinog.* **52**, 167–182 (2013).
14. Ma, S., Lee, T. K., Zheng, B. J., Chan, K. W. & Guan, X. Y. CD133+ HCC cancer stem cells confer chemoresistance by preferential expression of the Akt/PKB survival pathway. *Oncogene* **27**, 1749–1758 (2008).
15. Richardson, G. D. *et al.* CD133, a novel marker for human prostatic epithelial stem cells. *J. Cell. Sci.* **117**, 3539–3545 (2004).
16. Hermann, P. C. *et al.* Distinct populations of cancer stem cells determine tumor growth and metastatic activity in human pancreatic cancer. *Cell. Stem Cell.* **1**, 313–323 (2007).
17. Krohn, A. *et al.* CXCR4 receptor positive spheroid forming cells are responsible for tumor invasion in vitro. *Cancer Lett.* **280**, 65–71 (2009).
18. Hu, L. *et al.* Association of Vimentin overexpression and hepatocellular carcinoma metastasis. *Oncogene* **23**, 298–302 (2004).
19. Mani, S. A. *et al.* The epithelial-mesenchymal transition generates cells with properties of stem cells. *Cell* **133**, 704–715 (2008).
20. Elshamy, W. M. & Duhe, R. J. Overview: cellular plasticity, cancer stem cells and metastasis. *Cancer Lett.* **341**, 2–8 (2013).
21. Ray, P., De, A., Min, J. J., Tsien, R. Y. & Gambhir, S. S. Imaging tri-fusion multimodality reporter gene expression in living subjects. *Cancer Res.* **64**, 1323–1330 (2004).
22. Ganapathy-Kanniappan, S. *et al.* Human hepatocellular carcinoma in a mouse model: assessment of tumor response to percutaneous ablation by using glyceraldehyde-3-phosphate dehydrogenase antagonists. *Radiology* **262**, 834–845 (2012).

Acknowledgments

Author contributions

R.K. and S.G.-K. provided the original concept for the research and designed the study. R.K., S.K., E.K., D.F. and S.G.-K. performed experiments. M.L. analysed the animal imaging data. R.K., S.K., J.-F.G., E.K., M.L., D.F. and S.G.-K. discussed the results, prepared the manuscript. All authors reviewed the manuscript.

Additional information